Biomacromol. J., Vol.12, No.,2, July 2026.

Biomacromolecular Journal

www.bmmj.org

Cysteine–Reduced Graphene Oxide as a Nano-platform for Enhancing Glucose Oxidase Electron Transferring and Glucose Biosensing

Hedieh Naseri-Moghadam[1,2], Leila Shahriary[1], Hessam Sepasi Tehrani[1,3], Hedayatollah Ghourchian[1*]

[1]*Laboratory of Bioanalysis, Institute of Biochemistry & Biophysics, University of Tehran, P.O. Box 13145-1384, Tehran, Iran*

[2]*Department of Cell and Molecular Biology, Kharazmi University, Tehran, Iran*

[3]*Department of Biology, Science and Research Branch, Islamic Azad University, Tehran, Iran*

(Received 9 February 2026, Accepted 14 July 2026)

ABSTRACT

This study investigates the direct electron transfer of glucose oxidase (GOx) at a cysteine–reduced graphene oxide (rGO) nanocomposite formed on a glassy carbon electrode. The modified electrode was applied as an electrochemical biosensor for monitoring glucose levels. The proposed nanocomposite provides a favorable microenvironment to preserve the bioactivity of GOx. This immobilization strategy involves connection of GOx to rGO via L-cysteine (Cys) as the cross-linker. The GOx/Cys/rGO nanocomposite enabled the evaluation of the modified electrode as a sensitive biosensor for glucose detection. Under the experimental conditions, GOx showed an apparent Michaelis-Menten constant (Km) of 2.77 μM, indicating strong substrate binding. Glucose was detected in the concentration range from 1 to 8 μM with a detection limit of 3.6 nM and sensitivity of 603 μA mM^{-1} cm^{-2}. These findings highlight the potential of cysteine-functionalized reduce graphene oxide as a versatile nano-platform for high-performance glucose biosensors. The suggested strategy can be extended to other oxidase-based biosensing systems, emphasizing its broad applicability in electroanalysis and biomedical diagnostics.

Keywords: Nano-platform, Reduced graphene oxide, Cysteine, Biosensor, Glucose oxidase

INTRODUCTION

The determination of glucose is of paramount importance in industry, clinical diagnostics, environmental monitoring, and food processing. Regular and accurate monitoring of blood glucose level is crucial for effective disease management [1,2]. Glucose biosensors, which account for about 85% of the global biosensor market, are dominated by amperometric enzyme

electrodes based on glucose oxidase (GOx). These sensors have played a leading role in enabling blood sugar testing and are expected to support the development of continuous glucose monitoring systems [3–10]. Among the physical transducers used for biosensors, electrochemical methods offer inherent advantages such as simplicity, high sensitivity, good selectivity, easy integration, and relatively low cost [4-5,9-12]. Nanoscale materials have been widely utilized in biosensor design to enhance performance through improved electron transfer and increased surface area [4-8,11,13-16].

Graphene, a two-dimensional honeycomb network of sp^2-hybridized carbon atoms, possesses unique, electrical, optical, and structural properties. Its high surface area, excellent conductivity, and ease of functionalization make it an ideal platform for biosensor applications [17]. Graphene has been extensively studied for use in analytical chemistry, bioimaging, catalysis, and photovoltaic devices [18-21]. Recent studies have demonstrated that graphene-based nanocomposites significantly enhance the electrochemical performance of GOx biosensors, improving both sensitivity and stability [22]. Moreover, surface modification strategies including polymeric coatings can improve biosensor responsiveness and reproducibility [23]. Despite these advancements, challenges such as enzyme instability, limited sensitivity, and poor reproducibility still hinder the performance of GOx–graphene biosensors [24]. In addition to improving enzyme immobilization, amino acid-assisted functionalization of graphene-based materials has recently attracted considerable attention because it can provide favorable enzyme orientation, preserve biological activity, and facilitate direct electron transfer between the enzyme active center and the electrode surface. To address these limitations, this study introduces a cysteine-functionalized reduced graphene oxide nanocomposite that facilitates strong enzyme binding and efficient electron transfer. L-cysteine (Cys, $HS–CH_2–CH(NH_2)–COOH$), an amino acid with thiol, amino, and carboxyl functional groups, plays a crucial role in protein immobilization and self-assembly on electrode surfaces. It is widely used for covalent attachment of biomolecules to metal and functionalized insulating surfaces. The proposed mechanisms of Cys attachment to reduced graphene oxide involve interactions through its three functional groups [25]. Cys has been detected via various analytical methods [26] and electrochemically through oxidation reaction on electrode surface [27, 28]. The thiol group (-SH group) of Cys is oxidized, and two molecules are absorbed onto the electrode surface, leading to formation of Cys. Under high positive potential, this product can be further oxidized to cysteic acid [25].

Although Cys can be slightly electrodeposited onto bare glassy carbon electrode, its self-assembly does not occur readily without a facilitating matrix [17]. Therefore, the novelty of this work lies in employing Cys as a molecular linker to construct a stable GOx/Cys/rGO interface, which simultaneously enhances enzyme immobilization, facilitates direct electron transfer, and improves glucose sensing performance. Therefore, we propose that reduced graphene oxide (rGO) acts as a facilitator for the organized assembly of Cys and GOx on the electrode surface. Accordingly, a glucose oxidase/cysteine/rGO (GOx/Cys/rGO)

nanocomposite film was synthesized and applied for glucose sensing which exhibited superior sensitivity compared to other reduced graphene oxide-based systems.

MATERIALS AND METHODS

Chemical and reagent

GOx type II from Aspergillus Niger (EC 1.1.3.4,), β-D (+) glucose and L-cysteine were purchased from Sigma (U.S.A) and were used without further purification. K_3 [Fe $(CN)_6$], KCl, KH_2PO_4 and K_2HPO_4 were obtained from Merck. The glucose stock solution was stored overnight at room temperature before use.

Synthesis of Graphene Oxide and rGO

Graphene oxide (GO) was synthesized from graphite powder using a modified Hummer's method [29]. In brief, 1 g of graphite and 0.5 g of sodium nitrate ($NaNO_3$) were mixed up, followed by the gradual addition of 23 mL of concentrated sulfuric acid (H_2SO_4) under constant stirring. After 1 hour, 3 g of potassium permanganate ($KMnO_4$) was gradually added while maintaining the temperature below 20 °C to inhibit overheating and probable hazards. The reaction mixture was then stirred at 35 °C for 12 hours. Subsequently, 500 mL of deionized water was added under vigorous stirring to dilute the solution. To confirm complete reaction of $KMnO_4$, 5 mL of 30% hydrogen peroxide (H_2O_2) was added further. The resulting suspension was washed in sequence with hydrochloric acid (HCl) and deionized water, followed by filtration and drying. The final product consisted of GO sheets. rGO was prepared according to the method reported by Leila Shahriary et al. [30]

Electrode preparation

The glassy carbon electrode (GCE) was polished with 0.3 and 0.05 μm alumina slurry, followed by sequential sonication in absolute ethanol and double-distilled water for 1 min each. A 4 μL aliquot of reduced graphene oxide aqueous dispersion was drop-cast onto the cleaned GCE and allowed to dry at room temperature. The electrode was then immersed in phosphate buffer (pH 7.0) containing 5.0×10^{-3} mol L^{-1} Cys, and 20 cyclic voltammetry cycles were recorded between -0.7 and +1.7 V at a scan rate of 0.10 Vs^{-1} to ensure uniform and stable formation of the Cys layer on the electrode surface.

Enzyme modification of electrode

GOx was immobilized onto the Cys/rGO - modified glassy carbon electrode (GCE) via physical adsorption. Cys/rGO/GCE was incubated in an enzyme solution (1 mg/mL GOx in phosphate buffer, pH 7.0) at 4 ℃ for 12 h. Subsequently, the modified electrode was rinsed with phosphate buffer solution and stored at 4 ℃ until use.

Characterization technique

The surface morphology of the samples was examined using scanning electron microscopy (SEM, JEOL JSM-6360). Electrochemical measurements were conducted using an EG&G model 263A potentiostat/galvanostat controlled by a Power Suite software package and a GPIB interface. Electrochemical investigations were conducted in a conventional three-electrode cell, consisting of the glassy carbon electrode (GCE, from Azar Electrode, Uromia, Iran), an Ag/AgCl (3 M KCl solution) reference electrode (from Metrohm), and a platinum wire as a counter electrode. All measurements were carried out at room temperature under ambient conditioning. Prior to modification, GC electrodes were polished with 0.3 and 0.05 μm alumina slurry and rinsed thoroughly with Milli-Q water.

RESULTS AND DISCUSSION

Material characterization

The surface morphologies of the synthesized GO and rGO were characterized using SEM. The SEM image of GO (Figure 1a) reveals randomly aggregated, wrinkled sheets connected with each other. In contrast, the SEM image of rGO (Figure 1b) exhibits thinner, more transparent wrinkled sheets with a fluffy and roughly stacked structure, indicating successful reduction of GO.

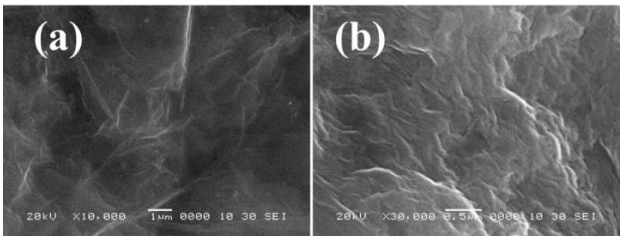

Figure 1. The SEM image of GO (a) and rGO (b)

Electrochemical investigations

pH Effect

To investigate the effect of pH on the electrochemical behavior of immobilized GOx, a series of experiments were carried out. Figure 2A displays peak currents of the electrode in phosphate buffer solution at various pH values ranging from 6.2 to 7.6. As the pH increased, both the anodic and cathodic peak potentials displayed a negative shift. The detected negative shift in both oxidation and reduction peak potentials with increasing pH confirms the participation of protons in the electron transfer process of the FAD/$FADH_2$ redox couple. This behavior follows the electrochemical mechanism where the formal potential ($E^{0\prime}$) is pH-dependent according to the Nernst equation for a system involving equal numbers of protons and electrons. The shift of nearly -62 mV per pH unit shows that the electron transfer is coupled with protonation/deprotonation of the enzyme's active site, maintaining the overall charge equilibrium during the redox process.

As illustrated in Figure 2B, the cathodic peak current increased as the pH changed from 6.2 to 7.0, followed by a decrease up to pH 7.6. The maximum cathodic peak current observed at pH 7.0 recommends this value signifies the optimum compromise between enzyme activity and stability. This pH is adjacent to the physiological optimal for natural GOx, indicating that the cysteine-rGO nanocomposite successfully preserves the enzyme's natural conformation and catalytic efficiency. The decrease in peak current beyond pH 7.0 may be attributed to partial denaturation of the enzyme or changes in the ionization states of critical amino acid residues in the enzyme's active site, thereby reducing electron transfer efficiency. Based on this plot, pH 7.0 was chosen as the optimal value for the subsequent experiments. This observation is consistent with the optimum catalytic activity of glucose oxidase under physiological conditions, indicating that the Cys/rGO nanocomposite effectively preserves the native conformation and electrochemical activity of the enzyme. As shown in Figure 2C, the formal potential ($E^{0\prime}$) exhibited a linear dependence on pH in the range of 6.2 to 7.8. The slope of the $E^{0\prime}$ versus pH plot was determined to be 0.062 V/pH from the linear regression equation $E^{0\prime} = -0.062(pH) - 0.023$. This slope approximates the theoretical Nernstian value of 0.059 V/pH, as expected for a reversible two-proton, two-electron transfer process at 25 °C.

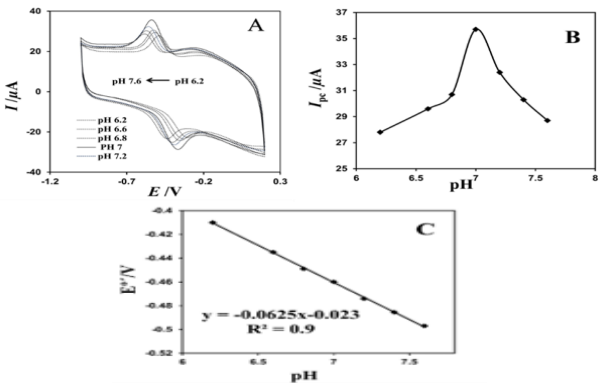

Figure 2. (A) CVs of GOx/Cys/rGO/GCE in 0.1 M phosphate buffer solution at different pHs; from right to left: 6.2, 6.6, 6.8, 7.0, 7.2, 7.4, and 7.6. The plots of Ipc versus pH and $E^{o\prime}$ versus pH are shown in (B), and (C), respectively.

Eectrochemical behavior of immobilized GOx on modified electrode

The electrochemical performance of GOx immobilized on the Cys/rGO/GCE was studied using cyclic voltammetry. Figure 3 shows CVs of different modified electrodes in 0.1 M phosphate buffer solution, pH 7.0 at the scan rate of 0.05 V. s^{-1}. No distinct electrochemical redox peaks were observed at the bare GCE (Curve A), agreeing with the absence of electroactive species. In the same way, the rGO/GCE (Curve B) showed no significant faradic response due to the lack of electroactive species. In contrast two well-defined quasi-reversible redox peaks appeared at GOx/rGO/GCE (Curve C) and GOx/Cys/rGO/GCE (Curve D) which are attributed to the FAD/$FADH_2$ redox couple within the GOx protein structure. Notably, the GOx/Cys/rGO/GCE exhibited the anodic peak at -362 mV and a cathodic one at -531 mV (versus Ag/AgCl). The observed redox response is consistent with previously reported CVs for GOx immobilized on graphene-based electrode [31].

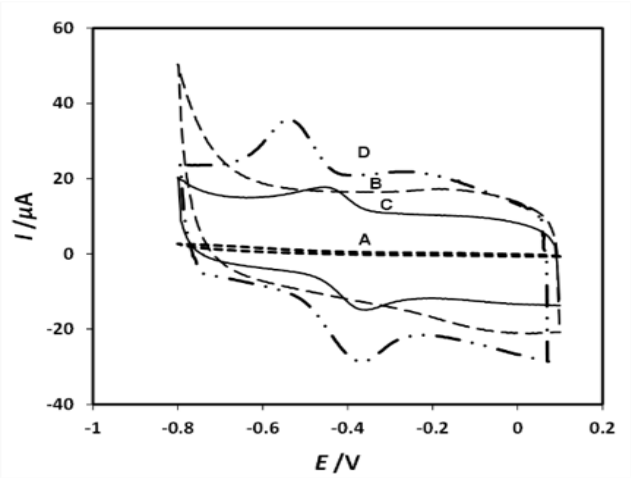

Figure 3. CVs of different modified electrodes: bare GCE (A), rGO/GCE (B), GOx/rGO/GCE (C) and GOx/Cys/rGO/GCE (D). The results were obtained in 0.1 M phosphate buffer solution, pH 7.0, at the scan rate of 50 mVs^{-1}.

The formal potential ($E^{o'}$) for GOx-modified electrode, calculated as the average of anodic (E_{pa}) and cathodic (E_{pc}) peak potentials, was -446.5 mV (versus Ag/AgCl). Obviously, the peak-to-peak separation (ΔEp) for GOx/Cys/rGO/GCE (169 mV), is greater than that observed for GOx/rGO/GCE (48 mV). This increased ΔEp value suggests that, while the Cys layer successfully facilitates enzyme immobilization and direct electron transfer, it introduces a modest kinetic barrier compared to direct adsorption on rGO. On the other hand, the well-defined redox peaks approve that efficient direct electron transfer is maintained through the Cys bridge, and the exceptional bio-sensing performance (sensitivity of 603 μA mM^{-1} cm^{-2}, limit of detection of 3.6 nM) demonstrate that this trade-off is favorable for practical biosensor applications.

The greater electrochemical response distinguished in the GOx/Cys/rGO/GCE can be due to the molecular bridging role of Cys. The thiol group of Cys forms a chemisorbed layer on rGO surface, whereas the amino and carboxyl groups facilitate ionic interactions with the enzyme. This configuration promotes efficient electron tunneling from the FAD redox center of GOx to the electrode surface, permitting direct electron transfer. The detected formal potential and peak separation further support the theory of a facilitated electron pathway over the cysteine–reduced graphene oxide interface. The presence of cysteine likely promotes a favorable orientation of GOx molecules on the rGO surface, reducing the electron tunneling distance between the FAD redox center and the conductive substrate.

The role of Cys/rGO nano-platform in enzyme electro transferring

In the present work, GOx was immobilized on the Cys-modified surface via incubating the enzyme solution (1 mg/mL in phosphate buffer

solution, at 4 °C) for 12 h (Scheme 1). However, based on the previously reported experimental results [32], although Cys can be electrodeposited onto a bare GCE, directly but its regular growth does not occur. It seems that rGO plays an important role in inducing the regular growth of Cys, leading to improve GOx assembly and therefore enhancing enzyme loading on the electrode surface. As reported earlier [28,33], rGO can readily form a thin film on the GCE surface through π–π electronic interactions. This occurs due to the two-dimensional network of sp^2-hybridized carbon atoms, whose surface provides active sites for π–π interactions as well as for the attachment of functional groups. This extremely conductive and large surface area provides an outstanding platform for the adsorption of small molecules such as cysteine. The thiol group (–SH) of cysteine can undergo oxidation on the rGO surface, leading to the formation of cystine or cystic acid. This process results in the formation of a chemisorbed layer on rGO [34,35]. Such a stable layer firmly ties up Cys to the rGO surface, thereby establishing a powerful interface for subsequent enzyme immobilization and electron transfer. Later Cys is anchored to the rGO surface through its thiol group, the amino ($–NH_2$) and carboxyl (–COOH) groups remain available. These functional groups can form ionic bonds with complementary residues in GOx, such as negatively charged carboxyl groups or positively charged amino groups of specific amino acids. Consequently, Cys reacts as a molecular bridge: one end binds strongly to rGO, while the other stabilizes the enzyme on the electrode surface [36]. This multipoint attachment ensures that GOx is in a firm orientation near to the conductive rGO interface. The short distance between the FAD/$FADH_2$ redox center and the electrode surface provides a more effective electron transfer pathway, thus improving the overall electrochemical performance of the biosensor [37]. Therefore, the Cys/rGO interface functions not only as an immobilization matrix but also as an efficient electron-transfer mediator, contributing to the enhanced electrochemical performance of the proposed biosensor.

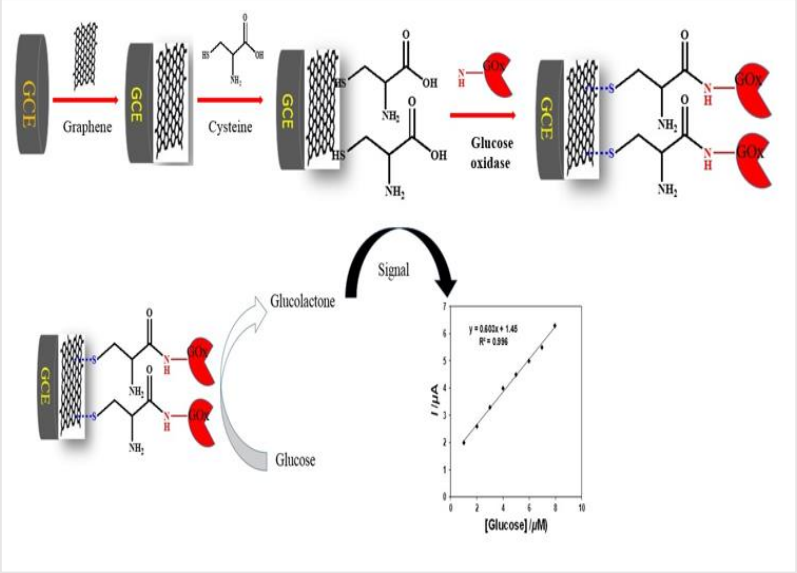

Scheme 1. Schematic representation of GOx immobilized on Cys/rGO/GCE.

Electrocatalytic activity of immobilized GOx

The electrocatalytic activity of GOx immobilized on Cys/rGO/GCE toward glucose was investigated. Figure 4A shows the CVs of the GOx/Cys/rGO/GCE in phosphate buffer solution.

The presence of oxygen is known to significantly affect the electrochemical characteristics of GOx, as documented in previous report [37]. Under the substrate-free condition (Curve A), the direct electron transfer of immobilized GOx can be described by Reaction 1:

$$\mathbf{GOx(FAD) + 2e^- + 2H^+ \overrightarrow{\longleftarrow} GOx\,(FADH_2)} \quad (\mathbf{1})$$

In oxygenated PBS without glucose, the enzyme's prosthetic group (FAD) remains oxidized due to Reaction 2 [38, 39].

$$\mathbf{GOx(FADH_2) + O_2 \longrightarrow GOx(FAD) + H_2O_2} \quad (\mathbf{2})$$

This reaction decreases the concentration of the reduced enzyme (GOx-FADH2) and increases the oxidized form (GOx-FAD). Consequently, at the electrode surface, the anodic peak current (Ipa) decreases while the cathodic peak current (Ipc) increased (Figure 4, Curve B).

Upon the addition of glucose to the oxygen-saturated PBS, (Curves b–g, Figure 4A), the cathodic peak current decreased. Glucose acts as a substrate for GOx and reduces the cathodic peak through two mechanisms: it converts FAD to $FADH_2$ (Reaction 3), thereby lowering the concentration of oxidized FAD, and it also consumes dissolved oxygen at the electrode surface (Reaction 4):

$$\mathbf{GOx(FAD) + Glucose \longrightarrow GOx\,(FADH_2) + Gluconolactone} \quad (\mathbf{3})$$

$$\mathbf{O_2 + Glucose \xrightarrow{GOx} Gluconolactone + H_2\,O_2} \quad (\mathbf{4})$$

These results exhibit that the Cys/rGO nanocomposite film not only established efficient electronic communication between the enzyme and the electrode but also preserves the electrocatalytic activity of GOx.

Figure 4B demonstrates the relationship between the changes in reduction peak current and the concentration. The electrode exhibited a linear response to glucose in the concentration range from 1 to 8 μM, with a sensitivity of 603 μA mM^{-1} cm^{-2}. The linear regression equation is y=0.603 x+1.45 (R=0.996), where y represents peak current (μA) and x stands for the glucose concentration (μM) (Figure. 4B inset).

These results exhibit that the Cys/rGO nanocomposite film not only established efficient electronic communication between the enzyme and the electrode but also preserves the electrocatalytic activity of GOx.

Figure 4B demonstrates the relationship between the changes in reduction peak current and the concentration. The electrode exhibited a linear response to glucose in the concentration range from 1 to 8 μM, with a sensitivity of 603 μA mM^{-1} cm^{-2}. The linear regression equation is y=0.603 x+1.45 (R=0.996), where y represents peak current (μA) and x stands for the glucose concentration (μM) (Figure. 4B inset).

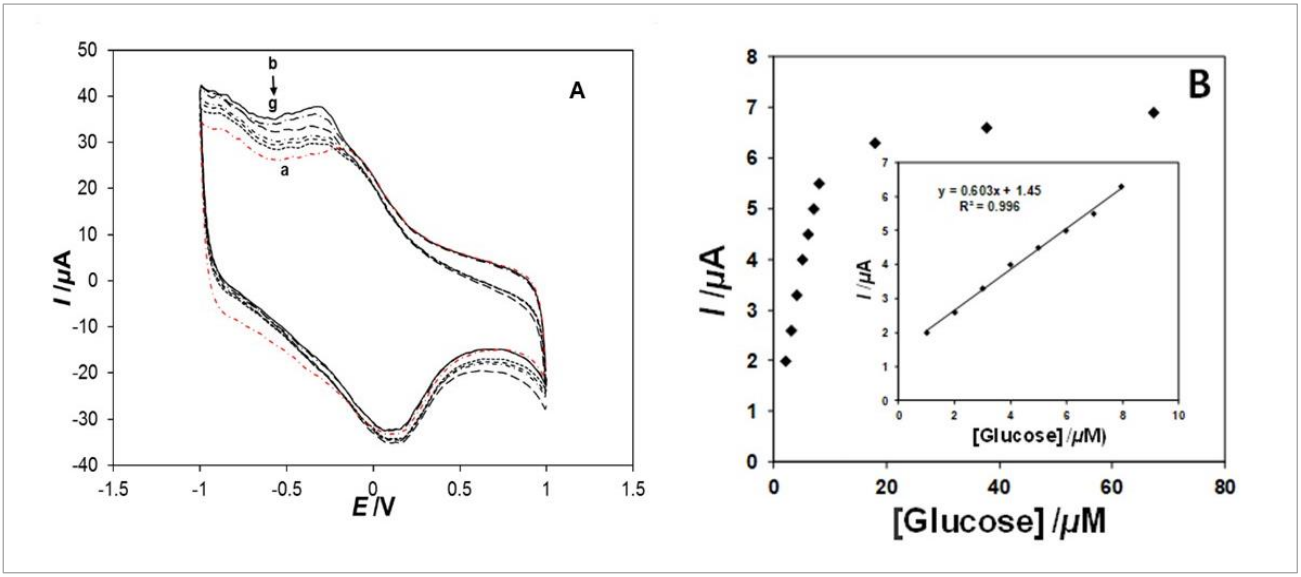

Figure 4. A: CVs of GOx/Cys/rGO/GCE in N_2 saturated phosphate buffer solution (a), and O_2 saturated phosphate buffer solution containing different glucose concentrations (from b to g: 0, 0.001, 0.004, 0.008, 0.067, and 0.658 mM). B: The calibration curve for glucose determination. Inset: The linear segment of calibration curve.

Limit of detection (LOD) of biosensor at signal/noise ratio of 3, was calculated to be 3.6 nM (Equation 1) [40]:

$$\mathbf{LOD=3\sigma/m} \qquad \mathbf{(1)}$$

Where, σ is standard deviation of background current (0.726 nA for 10 measurements near the LOD) and m is the slope of the calibration curve. To further demonstrate the analytical capability of the proposed biosensor, its performance was compared with representative graphene-based glucose biosensors reported in the literature. These results highlight the superiority of the nanocomposite for direct electrochemistry of GOx compared to other electrodes reported in the literature (Table 1). The improved analytical performance can be attributed to the collaborative effects of the highly conductive rGO network and the molecular bridging capability of cysteine, which together facilitate efficient electron transfer and maintain enzyme bioactivity.

Table 1. Comparison between the analytical parameters of the proposed electrode and other reported GOx/rGO based biosensors for glucose detection.

GOx/Gr based Nanocomposite	Linear Range	Detection Limit	Sensitivity (μA $mM^{-1}cm^{-2}$)	K_m^{ap}(M)	Reference
GOx/Gr	0.1-10mM	10±2 μM	110±3	-	[33]
GOx/IL-Gr[a]	2-16 mM	-	0.43	-	[42]
GOx/Gr/Chitosan	0.08-12 mM	20 μM	37.93	-	[43]
GOx/GQD[b]/CCE[c]	0.005-1.27 mM	1.73 μM	85	7.6×10^{-4}	[44]
rGO-ZnO	0.2-6.6 mM	0.2 μM	-	-	[45]
rGO-AgNPs	0.5-12.5 mM	0.16 mM	-	-	[46]
AuNPs-GR-CNTs	10 μm to 2 mM	4.1 mM	-	-	[47]
rGO-Cyclodextrin	50 μM to 3.0 mM	59.74 mM	-	-	[48]
PANI-SnO_2-rGO	0.1 nM to 5 mM	0.26 nM	-	-	[49]
Fe_3O_4–rGO	1 – 100 μM	0.32 μM	-	-	[50]
rGO-Fullerene-C60	0.1-12.5 mM	35 μM	-	-	[51]
ZrO_2-rGO	0.29–14 mM	≈ 290 μM	-	-	[52]
GOx/Cys/rGO	0.001-0.008 mM	0.0036 μM	603	2.89×10^{-6}	This work

[a]IL: Ionic liquid, [b]GQD: Graphene quantum dots, [c]CCE: carbon ceramic electrode

The relationship between the catalytic current and glucose concentration was analyzed using the electrochemical version of the Michaelis-Menten equation. The Lineweaver–Burk plot (Figure 5) was used to determine the kinetic parameters of the biosensor. The enzyme kinetic parameters, such as the apparent Michaelis-Menten constant (K_m^{ap}) and maximum current (I_{max}) under substrate-saturated conditions, were

calculated using the Lineweaver-Burk Equation 2 [41]:

$$1/I = 1/I_{max} + (K_m / I_{max})/C \quad (2)$$

Where I, shows the steady-state current and C is the glucose concentration. From the slope and intercept of the plot, K_m^{ap} and I_{max} were estimated to be 2.89 µM and 6.94 µA, respectively. The low K_m^{ap} value indicates a high biological affinity of the biosensor for glucose (Table 1).

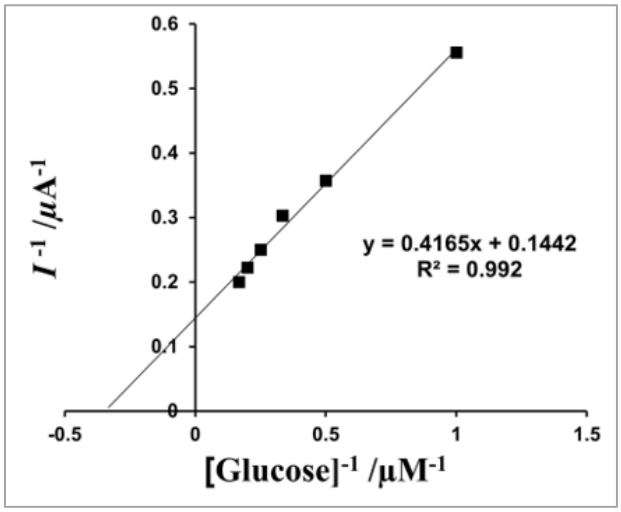

Figure 5. Lineweaver-Burk plot of GOx/Cys/rGO/GCE.

Comparing to the recent GOx–rGO biosensors reported in 2023 and 2024, the proposed GOx/Cys/rGO nanocomposite demonstrates superior analytical performance. For instance, Zhang et al. [53] developed a GOx–rGO–chitosan hybrid biosensor with a LOD of 12 nM and a sensitivity of 210 µA mM^{-1} cm^{-2}. In contrast, Harun-Or-Rashid et al. [54] reported a wearable sweat biosensor based on laser-induced rGO with a LOD of 47.7 µM and a sensitivity of 12.6 µA mM^{-1} cm^{-2}. While the present biosensor achieves a lower LOD (3.6 nM) and a markedly higher sensitivity (603 µA mM^{-1} cm^{-2}), underscoring the effectiveness of Cys as a molecular linker and rGO as a conductive material.

CONCLUSION

The Cys–rGO nanocomposite was successfully used for improvement of direct electron transfer of GOx. The nanocomposite provided a stable and conductive microenvironment that enhanced enzyme immobilization and preserved catalytic activity. The GOx/Cys/rGO/GCE exhibited a high sensitivity (603 µA mM^{-1} cm^{-2}), a low LOD (3.6 nM), and strong substrate affinity (K_m^{ap} = 2.89 µM), outperforming many previously reported GOx–rGO biosensors. It seems that rGO induces s regular growth of Cys, leading to enhance the enzyme loading on the electrode surface. The extremely conductive and large surface area rGO can readily form a thin film on the GCE through π–π interactions and provides an outstanding nano-platform for the adsorption of small molecules such as Cys. Such a stable layer establishes a powerful interface for subsequent enzyme immobilization and electron transfer. The amino ($–NH_2$) and carboxyl (–COOH) groups of Cys act as a multipoint molecular bridge between rGO and enzyme. This bridge may help that GOx places in a firm orientation for shortening the distance between FAD/$FADH_2$ redox center and conductive rGO interface providing an effective electron transfer pathway. These findings highlight the potential of Cys–rGO nanocomposite as a versatile nano-platform for developing high-performance electrochemical biosensors for clinical diagnostics and real-time glucose monitoring. The Cys/rGO platform might also be applicable to other redox

enzymes, extending its application in bio-sensing and bioelectronics.

ACKNOWLEDGMENTS

Financial support provided by the Research Council of the University of Tehran are gratefully appreciated.

REFRENCES

[1] K. Zhou, Y. Zhu, X. Yang, C. Li, Electroanalysis.22 (2010) 259–264

[2] S. Viswanathan,T.N. Narayanan, K. Aran, K.D. Fink, J.Paredes, P.M. Ajayan, S. Filipek, P. Miszta, H.C.Tekin, F. Inci, U. Demirci, P. Li, K.I. Bolotin, D. Liepmann, V. Renugopalakrishanan, Materials Today. 18 (2015) 513-522

[3] J. Wang, Chem. Rev.108 (2008) 814–825

[4] S. Yusan, M.M. Rahman, N. Mohamad, T.M. Arrif, A.Z.A. Latif, Journal of Analytical Methods in Chemistry. (2018)

[5] J.R. Anusha, C. JustinRaj, B.B. Cho, A.T. Fleming, K.H. Yu, B.C. Kim, Sensors and Actuators B: Chemical. 215 (2015) 536-543

[6] Y. Shao, J. Wang, H. Wu, J. Liu, I.A. Aksay, Y. Lin, Electroanalysis. 22 (2010) 1027–1036.

[7] Y. Liu, J. Zhang, Y. Cheng, S. P. Jiang, ACS Omega. 3 (2018) 667−676

[8] Y. Liu, X. Nan, W. Shi, X. Liu, Z. He, Y. Sun and D. Ge, RSC Adv. 9 (2019) 16439

[9] H. Zare, G.D. Najafpour, M. Jahanshahi, M. Rahimnejad, M. Rezvani, Romanian Biotechnological Letters. 22 (2017)

[10] M.A. Özbek, A. Yaşar, S. Çete, E. Er, N. Erk, J. Solid State Electrochem. 25 (2021) 1601–1610.

[11] E. Zor, Y. Oztekin, A. Ramanaviciene, Z. Anusevicius, H. Bingol, J. Barkauskas, M. Ersoz and A. Ramanavicius, J. Electrochem. Soc.161 (2014) 3064-3069

[12] M. Veerapandian,Y.T. Seo, H. Shin, K.Yun, M.H. Lee, Int.J. Nanomedicine. 7(2012) 6123–6136

[13] M. Thangamuthu, K.Y. Hsieh, P. V. Kumar and G.Y. Chen, Int. J. Mol. Sci. 20(2019) 2975

[14] N. S. Ridhuan, K. A. Razak, Z. Lockman, Scientific REPORTs. 8 (2018)13722

[15] A. Shamsazar, F.Shamsazar, A. Asadi, S. Rezaei-zarchi, Int. J. Electrochem. Sci. 11 (2016)9891 – 9901

[16] P. Rahimi, H. Ghourchian, H.A. Rafiee-Pour, P. Norouzi, M.R. GGanjali, Int.J. Electrochem. 2011 (2011) 7

[17] Y. Wang, Y.Shao, D.W. Matson, J. Li, Y. Lin, ACS Nano. 4 (2010) 1790–1798

[18] Y. Liu, X. Dong, P. Chen, Chem. Soc. Rev.41 (2012) 2283-2307

[19] K.S. Novoselov, A.K. Geim, S.V. Morozov, D. Jiang, Y. Zhang, S.V. Dubonos, I.V. Grigorieva, A.A. Firsov, Science. 306 (2004) 666-669

[20] Y. Zhu, S. Murali, W. Cai, X. Li, J.W. Suk, J.R. Potts, R.S. Ruoff, Adv. Mater. 22 (2010) 3906–3924

[21] S.G. Hong, J.H. Kim, R.E. Kim, S.J. Kwon, D.W. Kim, H.T Jung, J.S. Dordick, J. Kim, Biotechnol. Bioprocess Eng. 21 (2016) 573-579

[22] T. Alam, A. Das, Biosensors: Developments, Challenges and Perspectives, Springer Tracts in Electrical and Electronics Engineering, Springer (2024) 147–157.

[23] Y.N. Ning, B.L. Xiao, N.N. Niu, A.A. Moosavi-Movahedi, J. Hong, Sensors. 11 (2023) Article 3209.

[24] Z. Zhang, L. Huang, Y. Chen, Z. Qiu, X. Meng, Y. Li, RSC Adv. 14 (2024) 1034–1050.
[25] Z. Zhang, H. Jia, F. Ma, P. Han, X. Liu, B. Xu, J. Mol. Model. 17 (2011) 649–655
[26] S. Basu, X. Wang, M.T. Gladwin, D.B. Kim-Shapiro, Methods Enzymol. 440 (2008) 137-156
[27] P.T. Lee, D. Lowinsohn, R.G. Compton, Analyst. 139 (2014) 3755-3762
[28] A. Silva Fde, M.G. da Silva, P.R. Lima, M.R. Meneghetti, L.T. Kubota, M.O. Goulart, Biosens. Bioelectron. 50 (2013) 202-209
[29] L. Shahriary, A.A. Athawale, Int. J. Renew. Energy Environ. Eng. 2 (2014) 58–63.
[30] L. Shahriary, A. Athawale, Bull. Mater. Sci. 38 (2015) 739–745
[31] K. Eskandari, S. Sajjadi, A.H. Keihan, M. Kamali, J. Rashidiani, J. Appl. Biotechnol. Rep. 1 (2014) 77–80.
[32] G. Wang, H. Huang, G. Zhang, X. Zhang, B. Fang, L.Wang, Analytical Methods. 2 (2010)1692-1697
[33] P. Wu, Q. Shao, Y. Hu, J. Jin, Y. Y. Yin, H. Zhang, C. Cai, Electrochim. Acta 55 (2010) 8606-8614
[34] C.A. Martínez-Huitle, M. Cerro-Lopez, M.A. Quiroz, Mater. Res. 12 (2009) 375-384
35. F. Hua, T. Yao, Y. Yao, Sensors. 24 (2024) 1789.
[36] H. Sahebalzamani, K. Mehrani, H.R. Madaah Hosseini, K. Zare, J. Supercond. Nov. Magn. 32 (2019) 1299–1306.
[37] T. Yoon, W. Park, J. You, S. Na, Nanomaterials. 14 (2024) 1073.
[38] D. Wang, L. Chen, Electrochim. Acta.54 (2009) 4316-4320
[39] X. Wu, F. Zhao, J.R. Varcoe, A.E. Thumser, C. Avignone-Rossa, R.C. Slade, Bioelectrochemistry. 77 (2009) 64-68
[40] D.A. Skoog, F.J. Holler, T.A. Nieman, (1998) Principles of Instrumental Analysis. Brooks-Cole, Toronto
[41] R.A. Kamin, G.S. Wilson, Anal. Chem.52 (1980) 1198–1205
[42] Y. Jiang, Q. Zhang, F. Li, L. Niu, Sens. Actuators, B: Chemical. 161 (2012) 728-733
[43] X. Kang, J. Wang, H. Wu, I.A. Aksay, J. Liu, Y. Lin, Biosens. Bioelectron. 25 (2009) 901-905
[44] H. Razmi, R. Mohammad-RRezaei, Biosens Bioelectron.41(2013) 498-504
[45] R.S. Dey, C.R. Raj, RSC Adv. 3 (2013) 25858–25864
[46] S. Palanisamy, C. Karuppiah, S.M. Chen, Biointerfaces. 114 (2014) 164–169.
[47] R. Devasenathipathy, V. Mani, S.M. Chen, S.T. Huang, T.T. Huang, C.M. Lin, K.Y. Hwa, T.Y. Chen, B.J. Chen, Enzyme. Microbe. Technol. 78 (2015) 40–45.
[48] S. Palanisamy, R. Devasenathipathy, S.M. Chen, M. Ajmal Ali, C. Karuppiah, V. Balakumar, P. Prakash, M.S. Elshikh, F.M. Al-Hemaid, Electroanalysis. 27 (2015) 2412–2420
[49] S. Wu, F.Su, X. Dong, C. Ma, L. Pang, D. Peng, M. Wang, L. He, Z. Zhang, Appl. Surf. Sci.401 (2017) 262–270
[50] J. Shen, S. Shang, X. Chen, D. Wang, Y. Cai, Mater. Sci. Eng. C 76 (2017) 398–405.
[51] B. Thirumalraj, S.Palanisamy, S.M.Chen, C.Y. Yang, P. Periakaruppan, B.S. Lou, RSC Adv.5(2015)77651–77657.
[52] A.E. Vilian, S.M.Chen, M.A. Ali, F.M. Al-Hemaid, RSC Adv. 4(2014) 30358–30367.
[53] Y. Zhang, G. Guoqiang, Q. Liang, Y. Zani, P. Wang, F. Kang, Z. Liu, Z. Xue, Q. Li, B. Zhang, Front. Chem. 13 (2025) 1591302.
[54] M. Harun-Or-Rashid, N. Aktar, V. Preda, N. Nasiri, Sens. Diagn. 3 (2024) 893–913.